TIPE3 promotes non-small cell lung cancer progression via the protein kinase B/extracellular signal-regulated kinase 1/2-glycogen synthase kinase 3β-β-catenin/Snail axis

Qiang Li[1,2#], Dongmei Yu[1#], Zhengyuan Yu[1#], Qian Gao[1], Ruifang Chen[1], Lin Zhou[1], Rong Wang[1], Yan Li[3], Yulan Qian[1], Jun Zhao[4], Rafael Rosell[5,6], Min Tao[1], Yufeng Xie[1^], Chun Xu[4]

[1]Department of Oncology, the First Affiliated Hospital of Soochow University, Suzhou, China; [2]Department of Chemotherapy, Jiangxi Cancer Hospital of Nanchang University, Nanchang, China; [3]Department of Oncology, Suzhou Ninth People's Hospital, Suzhou, China; [4]Department of Cardio-Thoracic Surgery, the First Affiliated Hospital of Soochow University, Suzhou, China; [5]Catalan Institute of Oncology, Badalona, Spain; [6]Cancer Biology and Precision Medicine Program of the Germans Trias i Pujol Research Institute, Badalona (IGTP), Barcelona, Spain

Contributions: (I) Conception and design: C Xu, Y Xie, M Tao, Q Li, D Yu; (II) Administrative support: C Xu, Y Xie, M Tao; (III) Provision of study materials or patients: C Xu, Y Xie, M Tao; (IV) Collection and assembly of data: Q Li, D Yu; (V) Data analysis and interpretation: Y Xie, D Yu, Z Yu; (VI) Manuscript writing: All authors; (VII) Final approval of manuscript: All authors.

[#]These authors contributed equally to this work.

Correspondence to: Dr. Chun Xu. Department of Cardio-Thoracic Surgery, the First Affiliated Hospital of Soochow University, No. 188 Shizi Street, Suzhou 215006, China. Email: xuchun@suda.edu.cn; Prof. Yufeng Xie. Department of Oncology, the First Affiliated Hospital of Soochow University, No. 188 Shizi Street, Suzhou 215006, China. Email: sdxyf@163.com; Dr. Min Tao. Department of Oncology, the First Affiliated Hospital of Soochow University, No. 188 Shizi Street, Suzhou 215006, China. Email: taomin@suda.edu.cn.

Background: Tumor necrosis factor-α-induced protein 8-like 3 (TNFAIP8L3, also called TIPE3) has been shown to activate PI3K-AKT and MEK-ERK pathways. However, the roles of TIPE3 in progression of lung cancer are largely unknown.

Methods: Immunohistochemistry and western blotting were carried out to analyze the expression of TIPE3 in lung cancer clinical tissues and cells. TIPE3-overexpressing and knock-down NSCLC cell lines were established by transfer of TIPE3 coding sequence and shRNA, respectively. *In vitro* functional assays were performed to assess the effects of TIPE3 on proliferation and metastasis of NSCLC cells. Tumor xenograft mouse model was used to examine the roles of TIPE3 in growth of NSCLC cells *in vivo*. Western blotting, immunofluorescence, and immunohistochemistry were conducted to evaluate the association of TIPE3 and molecules related to AKT/ERK1/2-GSK3β-β-catenin/Snail pathway. PI3K, MEK, or GSK3β kinase and proteasome inhibition assays as well as β-Trcp and STUB1 siRNA assays were employed to determine the contribution of AKT/ERK1/2-GSK3β signaling and ubiquitin-proteasome pathway to the regulatory effects of TIPE3 on expression of β-catenin, Snail1, and Slug.

Results: We demonstrated that TIPE3 was elevated in lung cancer tissues and cells. The expression level of TIPE3 was positively correlated with malignant clinicopathological characteristics of lung cancer patients, such as tumor size, pathologic stage, and lymph node metastasis. Knockdown of TIPE3 suppressed the proliferation and growth of NSCLC cells as well as their migration and invasion ability, whereas TIPE3 overexpression facilitated these biological processes. Mechanistic data showed that TIPE3 promoted AKT and ERK1/2 signaling, inactivated GSK3β activity, and enhanced the expression and transcriptional activity of β-catenin, Snail1, and Slug in NSCLC cells. Kinase or proteasome inhibition and β-Trcp or STUB1 knockdown assays further revealed that TIPE3 upregulated β-catenin, Snail1, and Slug via the AKT/ERK1/2-GSK3β pathway, in an ubiquitin-proteasome-dependent manner. More importantly, clinical data demonstrated that the expression level of TIPE3 was positively associated with the activation of AKT/

^ ORCID: 0000-0003-0171-9458.

ERK1/2-GSK3β-β-catenin/Snail pathway in lung cancer.

Conclusions: Our findings indicate that upregulation of TIPE3 promotes the progression of human NSCLC considerably by activating β-catenin, Snail1, and Slug transcriptional signaling via the AKT/ERK1/2-GSK3β axis. Therefore, TIPE3 may represent a potential therapeutic target for NSCLC.

Keywords: Non-small cell lung cancer (NSCLC); tumor necrosis factor-α-induced protein 8-like 3 (TNFAIP8L3, also called TIPE3); proliferation and growth; metastasis; protein kinase B (AKT)/extracellular signal-regulated kinase 1/2 (ERK1/2)-glycogen synthase kinase 3β (GSK3β)-β-catenin/Snail axis

Introduction

Lung cancer is the leading cause of cancer-related death and has one of the fastest growing morbidity rates, especially in China (1-3). Non-small cell lung cancer (NSCLC) accounts for approximately 85% of all lung cancer cases. Treatment modalities for NSCLC include surgery, chemotherapy, radiotherapy, targeted therapy, immunotherapy, or combined therapy (4). Despite recent clinical advances in diagnosis and systematic therapy for NSCLC, the 5-year survival rate remains low for patients with this disease (1,2). Approximately 90% of NSCLC patients die due to complications related to tumor metastasis, which consistently poses a problem in prognosis and therapy of NSCLC patients (1,2). However, the mechanisms involved in NSCLC metastasis are complex and poorly understood. Therefore, elucidating the molecular mechanisms responsible for the progression and metastasis of NSCLC and identifying the potential therapeutic targets to improve treatment and prognosis for NSCLC patients are of paramount urgency.

The tumor necrosis factor-α-induced protein 8 (TNFAIP8/TIPE) family is a recently discovered group of highly homologous proteins that participate in various pathophysiological processes such as inflammation, infection, immunity, and cancer development (5-7). So far, four members of the TIPE family have been identified: TIPE, TNFAIP8-like 1 (TNFAIP8L1/TIPE1), TNFAIP8-like 2 (TNFAIP8L2/TIPE2), and TNFAIP8-like 3 (TNFAIP8L3/TIPE3) (5-7). A seminal study (8,9) demonstrated that TIPE3, a transfer protein of phosphatidylinositol 4,5-bisphosphate and phosphatidylinositol 3,4,5-trisphosphate, can enhance the activation of the phosphatidylinositol 3-kinase (PI3K)-protein kinase B (AKT) and mitogen-activated protein kinase kinase (MEK)-extracellular signal-regulated kinase (ERK) signaling pathways by regulating lipid metabolism. Consistently, TIPE3 activates AKT, ERK, and nuclear transcription factor-κB (NF-κB) signaling, thereby promoting malignant biological behaviors in NSCLC and breast cancer cells (10,11). TIPE3 can also inhibit p38 phosphorylation and impair p38 mitogen-activated protein kinase (MAPK) signaling by directly binding to p38, leading to apoptotic resistance in glioblastoma (12). More importantly, upregulation of TIPE3 in lung cancer, breast cancer, and glioblastoma is clinically associated with the presence of metastasis, a high T stage, and a poor prognosis (8,10-12). Interestingly, while TIPE3 is reduced in gastric cancer, the prognosis of gastric cancer patients with a high expression of TIPE3 is poor (13). Furthermore, in gastric cancer, TIPE3 promotes cell proliferation and metastasis via the PI3K-AKT pathway (13), whereas microRNA-9-5p (miR-9-5p) suppresses these processes by targeting TIPE3 (14). Accumulating evidence suggests that TIPE3 exhibits pro-oncogenic activity and may be required for carcinogenesis and cancer development. However, the functions and underlying mechanisms of TIPE3 in the progression of various cancers, including lung cancer, are largely unclear.

In the present study, we determined the expression of TIPE3 in a human lung cancer tissue microarray (TMA) containing 102 paired clinical lung cancer tumor (T) and adjacent non-tumor lung (N) tissues and in human NSCLC cell lines, and analyzed the clinical association between the expression level of TIPE3 and clinicopathological characteristics of lung cancer patients. TIPE3 expression was found to be significantly increased in lung cancer tissues and NSCLC cells, and was positively correlated with tumor size,

pathologic stage, and lymph node metastasis. We further assessed the biological role of TIPE3 in NSCLC cells and delineated its potential molecular mechanism by performing *in vitro* and *in vivo* loss- and gain-of-function assays. We demonstrated that TIPE3 promoted the growth and metastasis of NSCLC cells, and upregulated the expression levels of β-catenin, Snail1, and Slug via the AKT/ERK1/2-glycogen synthase kinase 3β (GSK3β) pathway. Our data, for the first time, show that TIPE3 positively modulates the signaling of β-catenin, Snail1, and Slug via the AKT/ERK1/2-GSK3β pathway in NSCLC cells, and TIPE3 promotes NSCLC progression via the AKT/ERK1/2-GSK3β-β-catenin/Snail axis. We present the following article in accordance with the MDAR reporting checklist (available at http://dx.doi.org/10.21037/tlcr-21-147).

Methods

Cell lines

The normal human bronchial epithelial cell line HBEpiC and a panel of human NSCLC cell lines including A549, H1975, H1299, and H292 were supplied by the Cell Bank of Type Culture Collection of Chinese Academy of Sciences (Shanghai, China). The cells were grown in Dulbecco's Modified Eagle Medium (DMEM; HyClone, Logan, UT, USA) containing 10% fetal bovine serum (FBS; Gibco, Gaithersburgh, MD, USA) and 100 U/mL penicillin-streptomycin antibiotics (Beyotime, Beijing, China).

Antibodies

Rabbit anti-TIPE3 (aa273-292) (cat. no. LS-C313352) for western blotting (WB) and immunohistochemistry (IHC) was purchased from LSBio (Seattle, WA, USA). Rabbit anti-p-AKT (Thr308, T308) (cat. no. AF3262), anti-p-AKT (Ser473, S473) (cat. no. AF0016), anti-AKT (cat. no. AF6261), anti-p-ERK1/2 (Thr202/Tyr204) (cat. no. AF1015), anti-ERK1/2 (cat. no. AF0155), anti-p-GSK3β (Ser9) (cat. no. AF2016), and anti-GSK3β (cat. no. AF5016) for WB, IHC, and immunofluorescence (IF) were obtained from Affinity (Cincinnati, OH, USA). Rabbit anti-β-catenin (cat. no. 8480) for WB, IF, and IHC, as well as anti-Snail1 (cat. no. 3879) and anti-histone H3 (cat. no. 9717) for WB, and anti-Slug (cat. no. 9585), anti-E-cadherin (cat. no. 3195), anti-N-cadherin (cat. no. 13116), and anti-vimentin (cat. no. 5741) for WB and IF, were purchased from CST (Danvers, MA, USA). Rabbit anti-Snail1 (cat. no. 101167-T10) for IF and IHC was supplied by Sino

Biological (Wayne, PA, USA), and rabbit anti-Slug (cat. no. GTX128796) for IHC was supplied by GeneTex (Irvine, CA, USA). Rabbit anti-cyclin D1 (cat. no. YT1173) for WB and IF was purchased from ImmunoWay (Plano, TX, USA), as were anti-β-actin (cat. no. YM3214) and horseradish peroxidase (HRP)-conjugated goat anti-rabbit IgG (cat. no. RS0002) for WB. Servicebio (Wuhan, Hubei, China) supplied the HRP-conjugated goat anti-rabbit IgG (cat. no. G1213) for IHC, and Abcam (Cambridge, MA, USA) supplied the Alexa Fluor 647-conjugated goat anti-rabbit IgG (cat. no. ab150079) used for IF.

Establishment of TIPE3-overexpressing and knock-down NSCLC cell lines

Lentivirus (LV) (lentiviral plasmid: pLenti6.3/IRES/GFP; packaging plasmids: pLP1, pLP2, and VSVG) carrying human TIPE3 short hairpin RNA (shRNA) 1# (shTIPE3 1#) (shTIPE3 1#-F: 5'-CAC CGC TCT ACA AAG TCA CCA AAG ACG AAT CTT TGG TGA CTT TGT AGA GC-3'; shTIPE3 1#-R: 5'-AAA AGC TCT ACA AAG TCA CCA AAG ATT CGT CTT TGG TGA CTT TGT AGA GC-3'), shTIPE3 2# (shTIPE3 2#-F: 5'-CAC CGC CAA GAG GAG CTG GTT ATT GCG AAC AAT AAC CAG CTC CTC TTG GC-3'; shTIPE3 2#-R: 5'-AAA AGC CAA GAG GAG CTG GTT ATT GTT CGC AAT AAC CAG CTC CTC TTG GC-3'), shTIPE3 3# (shTIPE3 3#-F: 5'-CAC CGC GCA TCA ACC ACG TCT TTA ACG AAT TAA AGA CGT GGT TGA TGC GC-3'; shTIPE3 3#-R: 5'-AAA AGC GCA TCA ACC ACG TCT TTA ATT CGT TAA AGA CGT GGT TGA TGC GC-3') or control shRNA (shcontrol) (shcontrol-F: 5'-CAC CGC TAC ACA AAT CAG CGA TTT CGA AAA ATC GCT GAT TTG TGT AG-3'; shcontrol-R: 5'-AAA ACT ACA CAA ATC AGC GAT TTT TCG AAA TCG CTG ATT TGT GTA GC-3'), as well as LV (lentiviral plasmid: pLenti6.3/shRNA/GFP; packaging plasmids: pLP1, pLP2, and VSVG) carrying the TIPE3 coding sequence (CDS) for 204aa (NM_001311175.2) (TIPE3$_{204aa}$-F: 5'-GAA GCT AGC GCC ACC ATG GAT TCG GAT TCC GGG GAG-3'; TIPE3-R: 5'-ATA GGC GCG CCT TAA AGG ACT TTC TCA TCT AG-3') or 292aa (NM_207381.3) (TIPE3$_{292aa}$-F: 5'-GAA GCT AGC GCC ACC ATG GGG AAA CCA CGG CAA AAC-3'; TIPE3-R: 5'-ATA GGC GCG CCT TAA AGG ACT TTC TCA TCT AG-3') and blank control LV were supplied by Novobio (Shanghai, China). All of the above LVs expressed green fluorescent protein (GFP) and blasticidin S deaminase. To generate the

TIPE3 knock-down NSCLC cell line, H1299 and H292 cells were infected with LV-shTIPE3 1#, LV-shTIPE3 2#, LV-shTIPE3 3#, or LV-shcontrol, and then selected with 10 µg/mL of blasticidin S (Yeasen, Shanghai, China). For the generation of the TIPE3-overexpressing NSCLC cell line, A549 cells were infected with LV-TIPE3$_{204aa}$, LV-TIPE3$_{292aa}$, or LV, and then selected with blasticidin S.

Cell Counting Kit (CCK)-8 assay

Cells were seeded into 96-well plates at a density of 4×10^3 cells/100 µL culture medium per well. After 1, 2, 3, and 4 days of culture, the proliferation ability of the cells was determined using a CCK-8 assay (Beyotime). The optical density (OD) value of each well was measured at 450 nm with an automatic microplate reader. The cell growth curve was plotted with OD value versus (*vs.*) culture time.

Colony-forming assay

Cells were dispensed into 6-well plates at a density of 800 cells/4 mL culture medium per well. After 3 weeks of culture, the cell colonies were fixed with 4% paraformaldehyde and stained with 0.5% crystal violet. The clonogenic ability of the cells was then analyzed.

Tumorsphere assay

Cells were added into 6-well ultra-low adherent plates at a density of 1×10^4 cells/4 mL MammoCult™ basal medium plus 10% MammoCult™ proliferation supplement (STEMCELL, Vancouver, BC, Canada) per well. After 1 week of incubation, the number of the tumor spheres was counted.

Cell cycle analysis

Cells (1×10^6 cells) were washed and fixed with ice-cold 70% ethanol at 4 ℃ overnight. Following that, the cells were washed and stained with propidium iodide (PI)/RNase Staining Buffer (BD, San Diego, CA, USA) in the dark at room temperature for 15 minutes. Finally, the cell cycle profile of the cells was analyzed by flow cytometry.

Wound healing assay

Cells (5×10^5 cells/4 mL culture medium per well) were seeded into 6-well plates. When the cells reached confluency, scratches were made and reference points were marked on the outer bottoms. The wells were then rinsed to remove cellular debris and loaded with DMEM containing 2% FBS to maintain cell growth. At 24 hours after wounding, the migratory ability of the cells was analyzed.

Transwell invasion assay

Cells (5×10^5 cells/100 µL serum-free DMEM per chamber) were seeded into the upper chamber of 24-well Transwell inserts with an 8-µm pore size (Merck Millipore, Billerica, MA, USA) precoated with Matrigel (BD), and 600 µL DMEM containing 10% FBS was placed into the lower chamber. After 24 hours of incubation, cells invading the bottom chamber were fixed with 4% paraformaldehyde and stained with 0.5% crystal violet. Finally, the invasion ability of the cells was analyzed.

Tumor xenograft mouse model

Cells (2×10^6 cells/100 µL phosphate-buffered saline (PBS) per mouse; six mice per group) were injected subcutaneously into 4-week-old athymic BALB/c nude mice (Shanghai SLAC Laboratory Animal Co., Ltd., Shanghai, China). Tumor growth was monitored through the assessment of tumor volume each week. Tumor volume was calculated using the following formula: volume=$ab^2/2$, a: longer diameter, b: shorter diameter. At 4 weeks after inoculation, the tumor-bearing mice were sacrificed, and the xenograft tumors were dissected and weighed. Tumor growth was further evaluated by tumor weight. The animal experiment was conducted in the animal facility at Soochow University (Suzhou, Jiangsu, China) under a project license (IRB no. A201809059) granted by Laboratory Animal Center of Soochow University, in compliance with its institutional guidelines for the care and use of animals.

Lung cancer TMA preparation

A total of 102 paired clinical T and N tissues were collected from 102 primary lung cancer patients who underwent surgery at the Department of Cardio-Thoracic Surgery of the First Affiliated Hospital of Soochow University (Suzhou) between January 2016 and April 2017. None of the patients had received neoadjuvant therapy. The tissues were snap-frozen and stored in liquid nitrogen or were fixed in 10% neutral formalin and embedded in paraffin. The paraffin-embedded specimens were then used to prepare a human

940

Li et al. TIPE3 accelerates NSCLC progression by AKT/ERK1/2-GSK3β-β-catenin/Snail pathway

lung cancer TMA with a sample diameter of 1.5 mm (102 cases, 102 pairs, 204 dots). All procedures performed in this study involving human participants were in accordance with the Declaration of Helsinki (as revised in 2013). Informed consent was taken from all the patients. This experiment was approved by the Ethics Committee of the First Affiliated Hospital of Soochow University (IRB No. 2021-036).

WB analysis

Total lysates from snap-frozen clinical tissues and cells, as well as nuclear lysates from cells, were subjected to enhanced chemiluminescence (ECL)-based WB analysis for the detection of TIPE3, p-AKT, AKT, p-ERK1/2, ERK1/2, p-GSK3β, GSK3β, β-catenin, Snail1, Slug, cyclin D1, E-cadherin, N-cadherin, vimentin, β-actin (loading control for total lysates), and histone H3 (loading control for nuclear lysates), as reported previously (15). The primary antibodies used were: rabbit anti-TIPE3 (1:1,000), anti-p-AKT (T308) (1:1,000), anti-p-AKT (S473) (1:1,000), anti-AKT (1:1,000), anti-p-ERK1/2 (1:1,000), anti-ERK1/2 (1:1,000), anti-p-GSK3β (1:1,000), anti-GSK3β (1:1,000), anti-β-catenin (1:1,000), anti-Snail1 (1:1,000), anti-Slug (1:1,000), anti-cyclin D1 (1:1,000), anti-E-cadherin (1:1,000), anti-N-cadherin (1:1,000), anti-vimentin (1:1,000), anti-β-actin (1:3,000), and anti-histone H3 (1:2,000). The secondary antibody used was HRP-conjugated goat anti-rabbit IgG (1:10,000).

IF analysis

Frozen, 3-μm-thick xenograft tumor sections were fixed in 4% paraformaldehyde, placed in Ethylene Diamine Tetraacetic Acid (EDTA) (pH =7.4) for antigen retrieval, and blocked with normal goat serum. Then, the sections were stained with a panel of primary antibodies specific for p-AKT (T308) (1:100), p-AKT (S473) (1:100), AKT (1:100), p-ERK1/2 (1:200), ERK1/2 (1:200), p-GSK3β (1:100), GSK3β (1:100), β-catenin (1:100), Snail1 (1:300), Slug (1:400), cyclin D1 (1:100), E-cadherin (1:200), N-cadherin (1:200), or vimentin (1:100). After incubation with Alexa Fluor 647-conjugated goat anti-rabbit IgG (1:1,000) secondary antibody, the sections were subjected to nuclear counterstaining using 4',6-diamidino-2-phenylindole (DAPI) and mounted with antifade mounting medium (Beyotime) to prevent fluorescence fading. Finally, fluorescence of the sections was observed under confocal microscopy.

Kinase and proteasome inhibition assays

TIPE3-overexpressing cells were pretreated with 10 μM of PI3K inhibitor LY294002 (APExBIO, Houston, TX, USA), 10 μM of MEK inhibitor PD98059 (APExBIO), or dimethyl sulfoxide (DMSO; vehicle control) for 1 hour. TIPE3 knock-down cells were pretreated with 25 μM of GSK3β inhibitor VIII (APExBIO), 10 μM of proteasome inhibitor MG132 (APExBIO), or DMSO (vehicle control) for 1 hour. The treated and unpretreated cells were cultured for another 24 hours and then harvested for WB detection of total and nuclear expression of β-catenin, Snail1, and Slug.

β-transducin repeat-containing protein (β-Trcp) and STIP1 homology and U-box-containing protein 1 (STUB1) siRNA assays

TIPE3 knock-down cells were transfected with 50 nM of β-Trcp small interfering RNA (siRNA) (siβ-Trcp), STUB1 siRNA (siSTUB1), or control siRNA (sicontrol) (RiboBio, Guangzhou, Guangdong, China) using HiPerFect transfection reagent (Qiagen, Hilden, Nordrhein-Westfalen, Germany). After 24 hours of transfection, the transfected and untransfected cells were subjected to WB analysis to detect the total and nuclear expression of β-catenin, Snail1, and Slug.

IHC analysis

A lung cancer TMA block was cut into 3-μm-thick sections for IHC detection of TIPE3, p-AKT, AKT, p-ERK1/2, ERK1/2, p-GSK3β, GSK3β, β-catenin, Snail1, and Slug, as described previously (15). The primary antibodies used were: rabbit anti-TIPE3 (1:100), anti-p-AKT (T308) (1:50), anti-p-AKT (S473) (1:50), anti-AKT (1:50), anti-p-ERK1/2 (1:50), anti-ERK1/2 (1:100), anti-p-GSK3β (1:50), anti-GSK3β (1:50), anti-β-catenin (1:100), anti-Snail1 (1:500), and anti-Slug (1:100). The secondary antibody used was HRP-conjugated goat anti-rabbit IgG (1:200). Expression levels were evaluated using a weighted IHC scoring system (0–1, –; 2–3, +; 4–5, ++; and 6–7, +++), with a weighted score of ≥4 (++ or +++) considered as high expression (15).

Statistical analyses

IHC scoring data were presented as –, +, ++ or +++. Categorical data of high or low expression were presented

as percentage of total cases. Measurement data of functional studies were tested for normal distribution and presented as mean ± standard deviation (SD) when P>0.1. Measurement data were further analyzed using a homogeneity of variance test, in which P>0.1 indicated homogeneity of variance, followed by analysis of variance (ANOVA). All statistical tests, including the Mann-Whitney U test, Pearson's χ^2 test, Student's t-test, and ANOVA with least significant difference (LSD) post-hoc multiple comparison, were performed with SPSS20.0 (SPSS, Chicago, IL, USA). A two-sided P value <0.05 was considered to indicate a statistically significant difference.

Results

TIPE3 expression was elevated in human lung cancer tissues and cells

To determine the expression of TIPE3 in lung cancer tissues, IHC staining of a human lung cancer TMA (102 paired T and N tissues) was performed. As shown in *Figure 1A*, compared with N control tissues, lung cancer T tissues exhibited a significantly higher expression level of TIPE3. High TIPE3 expression was observed in 57.8% of the T tissues (59 cases; 11 cases scored '+++' and 48 cases scored '++'), compared to only 32.4% of the N tissues (33 cases, with 3 cases scoring '+++' and 30 cases scoring '++') (P<0.05) (*Figure 1B,C*). WB analysis confirmed that TIPE3 expression was increased in lung cancer T tissues (*Figure 1D*). Our clinical data on the expression level of TIPE3 in lung cancer T tissues were consistent with those reported in previous studies (8,10). To evaluate the expression of TIPE3 in lung cancer cells, WB was performed to detect TIPE3 in the human NSCLC cell lines A549, H1975, H1299, and H292, and the normal human bronchial epithelial cell line HBEpiC. As shown in *Figure 1E*, NSCLC cells exhibited a higher expression of TIPE3 than the HBEpiC control cells (P<0.05). This result showed that TIPE3 was upregulated in human lung cancer tissues and cells.

Correlation of TIPE3 with clinicopathological features of lung cancer patients

According to the expression level of TIPE3 in lung cancer T tissues, the 102 lung cancer patients were divided into two groups: the low TIPE3 expression group (43 cases) and the high TIPE3 expression group (59 cases). The correlations of TIPE3 with clinicopathological variables of lung cancer

patients, including age, sex, histology, differentiation, tumor size, pathologic stage, and lymph node metastasis, were then analyzed. As shown in *Table 1*, high expression of TIPE3 was associated with large tumor size, high pathologic stage, and the presence of lymph node metastasis (P<0.05). Our results showed that the expression level of TIPE3 was positively correlated with malignant clinicopathological features of lung cancer patients, suggesting that TIPE3 may contribute to lung cancer progression.

Knockdown or overexpression of TIPE3 in human NSCLC cells

To generate TIPE3 knock-down lung cancer cells for loss-of-function assays, the NSCLC cell lines H1299 and H292 were infected with LV-shTIPE3 (1#, 2# or 3#) or LV-shcontrol (control). To generate TIPE3-overexpressing lung cancer cells for gain-of-function assays, the A549 NSCLC cell line was infected with LV-TIPE3 (204aa or 292aa) or LV (control). After selection with blasticidin S, the transgenic cells were identified by flow cytometry of GFP expression and WB analysis of TIPE3 expression. As shown in *Figure 2A*, over 90% of the LV-infected H1299, H292, and A549 cell derivatives expressed GFP, demonstrating extremely high transgene efficiency. WB analysis further confirmed that knockdown of TIPE3 in H1299 and H292 NSCLC cells (*Figure 2B*), as well as TIPE3 overexpression in A549 NSCLC cells expressing either TIPE3$_{204aa}$ or TIPE3$_{292aa}$ (*Figure 2C*), had been successfully established (P<0.05). Moreover, in both H1299 and H292 cells, the knockdown efficiency of TIPE3 elicited by LV-shTIPE3 1# was stronger than that elicited by LV-shTIPE3 2# or LV-shTIPE3 3# (*Figure 2B*). Therefore, H1299-LV-shTIPE3 1# (H1299-shTIPE3) *vs.* H1299-LV-shcontrol (H1299-shcontrol), H292-LV-shTIPE3 1# (H292-shTIPE3) *vs.* H292-LV-shcontrol (H292-shcontrol), and A549-LV-TIPE3$_{204aa}$ (A549-TIPE3$_{204aa}$) or A549-LV-TIPE3$_{292aa}$ (A549-TIPE3$_{292aa}$) *vs.* A549-LV (A549-mock) were used for the subsequent cell function assays.

TIPE3 accelerated human NSCLC cell proliferation and growth

To examine the effect of TIPE3 on human NSCLC cell growth *in vitro*, the proliferative ability of H1299-shTIPE3 *vs.* H1299-shcontrol, H292-shTIPE3 *vs.* H292-shcontrol, and A549-TIPE3$_{204aa}$ or A549-TIPE3$_{292aa}$ *vs.*
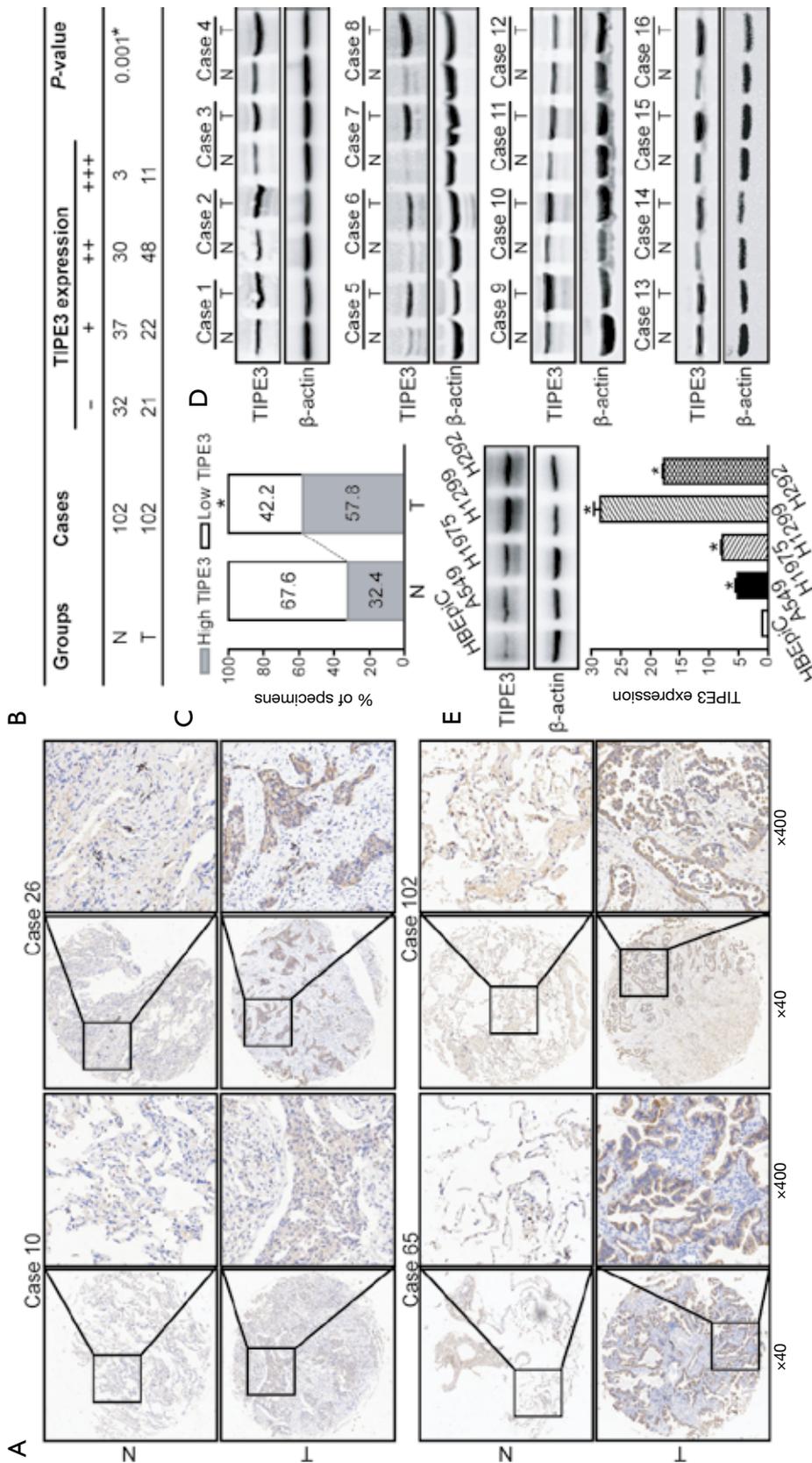
Figure 1 TIPE3 expression is elevated in lung cancer tissues and cell lines. (A,B,C) IHC analysis of TIPE3 in lung cancer TMA. (A) Representative IHC images of paired T and N tissues from four cases (T IHC score: Case 10, −; Case 26, +; Case 65, ++; and Case 102, +++). (B) The numbers of cases with IHC scores −, +, ++ or +++ for T and N tissues from 102 cases are shown. * , P<0.05, Mann-Whitney U test. (C) Percentage of T and N tissues with high (++ or +++) and low (− or +) TIPE3 expression is shown. * , P<0.05, Pearson's χ² test. (D) WB analysis of TIPE3 expression in lung cancer tissues. Representative WB images of paired T and N tissues from 16 cases. (E) WB analysis of TIPE3 expression in NSCLC cells. Representative WB images (upper) and relative protein level of TIPE3 in NSCLC cells (with HBEpiC as a control) (lower) are shown. * , P<0.05, ANOVA with LSD post-hoc multiple comparison, n=6 per group. IHC, immunohistochemistry; TMA, tissue microarray; T, lung cancer tumor; N, adjacent non-tumor lung; WB, Western blotting; NSCLC, non-small cell lung cancer; ANOVA, analysis of variance; LSD, least significant difference.

Table 1 Correlation of TIPE3 expression in lung cancer tissues with clinicopathological features of lung cancer patients

Variables	Low TIPE3 (n=43)	High TIPE3 (n=59)	P value
Age, years			
≤65	24	28	0.404
>65	19	31	
Sex			
Male	22	30	0.975
Female	21	29	
Histology			
Adeno	33	43	0.658
SCC/other	10	16	
Differentiation			
Well	6	2	0.113
Moderate/poor	37	57	
Tumor size			
T1	25	19	0.009*
T2/T3/T4	18	40	
Pathologic stage			
I/II	39	38	0.002*
III/IV	4	21	
Lymph node metastasis			
N0	36	33	0.003*
N1/N2	7	26	

*, $P<0.05$, Pearson's χ^2 test.

A549-mock tumor cells was analyzed using a CCK-8 assay. As shown in *Figure 3A*, knockdown of TIPE3 significantly inhibited H1299 and H292 tumor cell proliferation *in vitro*, whereas overexpression of either TIPE3$_{204aa}$ or TIPE3$_{292aa}$ promoted A549 tumor cell proliferation *in vitro* ($P<0.05$). Furthermore, colony-forming (*Figure 3B,C*) and tumorsphere (*Figure 3D,E*) assays showed that knockdown of TIPE3 resulted in the formation of small and few colonies or spheres in H1299 and H292 tumor cells, whereas overexpression of TIPE3 produced large and numerous A549 cell colonies or spheres ($P<0.05$), indicating that TIPE3 enhances the clonogenicity and self-renewal ability of NSCLC cells. Additionally, knockdown of TIPE3 induced G1-phase arrest and S-phase reduction in H1299 and H292 cells, whereas overexpression of TIPE3 facilitated G1-to-S phase transition in A549 tumor cells

($P<0.05$) (*Figure 3F,G*). To determine whether TIPE3 could also promote NSCLC cell growth *in vivo*, H1299-shTIPE3, H1299-shcontrol, H292-shTIPE3, H292-shcontrol, A549-TIPE3$_{292aa}$, and A549-mock tumor cells were subcutaneously injected into athymic BALB/c nude mice, and the tumor growth was tracked. Data from the *in vivo* xenograft model (*Figure 4*) showed that knockdown of TIPE3 also markedly suppressed tumor growth in mice injected with H1299 and H292 cells, whereas overexpression of TIPE3 accelerated tumor growth in the A549-bearing mice ($P<0.05$). Together, these data demonstrated that TIPE3 could promote NSCLC cell proliferation and growth *in vitro* and *in vivo*.

TIPE3 promoted NSCLC cell metastasis in vitro

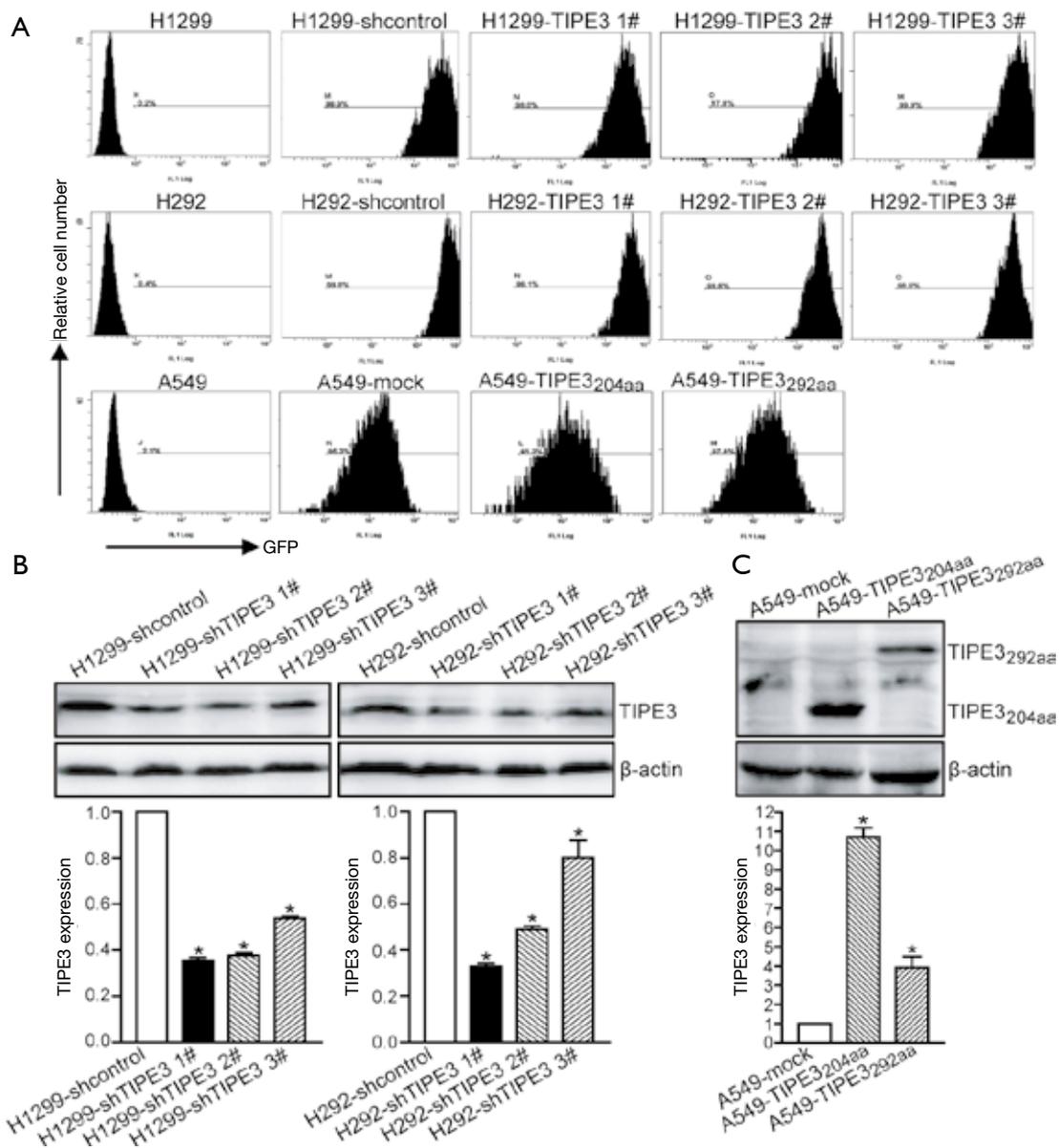To investigate the role of TIPE3 in NSCLC metastasis,

Figure 2 Knockdown or overexpression of TIPE3 in NSCLC cells. (A) Determination of transgene efficiency by flow cytometric analysis of GFP. (B) WB analysis of TIPE3 knockdown efficiency in H1299 and H292 cells. Representative WB images (upper) and relative protein level of TIPE3 in H1299-shTIPE3 cells (with H1299-shcontrol as a control) and H292-shTIPE3 cells (with H292-shcontrol as a control) (lower) are shown. *, P<0.05, ANOVA with LSD post-hoc multiple comparison, n=6 per group. (C) WB analysis of TIPE3 overexpression efficiency in A549 cells. Representative WB images (upper) and relative protein level of TIPE3 in A549-TIPE3$_{204aa}$ and A549-TIPE3$_{292aa}$ cells (with A549-mock as a control) (lower) are shown. *, P<0.05, ANOVA with LSD post-hoc multiple comparison, n=6 per group. NSCLC, non-small cell lung cancer; GFP, green fluorescent protein; WB, Western blotting; ANOVA, analysis of variance; LSD, least significant difference.

the migratory and invasive behavior of H1299-shTIPE3 *vs.* H1299-shcontrol, H292-shTIPE3 *vs.* H292-shcontrol, and A549-TIPE3$_{204aa}$ or A549-TIPE3$_{292aa}$ *vs.* A549-mock

tumor cells were analyzed using *in vitro* wound healing and Transwell invasion assays, respectively. Compared with that of H1299-shcontrol and H292-shcontrol cells, the
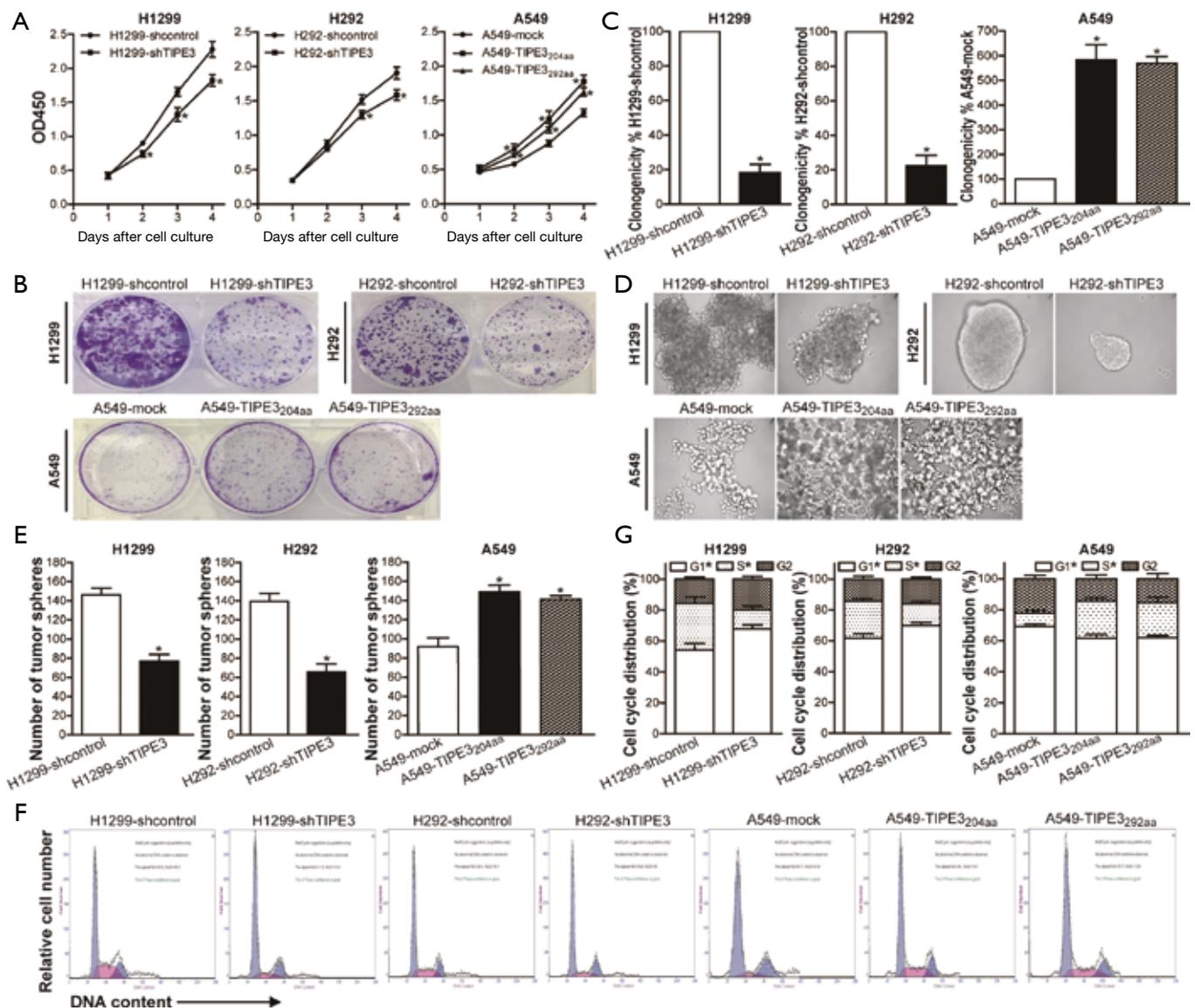
Figure 3 TIPE3 promotes proliferation, self-renewal and G1-to-S phase transition in NSCLC cells. (A) CCK-8 assay. *, P<0.05, ANOVA with LSD post-hoc multiple comparison, n=6 per group. (B,C) Colony-forming assay. Representative images of tumor colonies (B) and relative clonogenic ability of H1299-shTIPE3 cells (with H1299-shcontrol as a control) and H292-shTIPE3 cells (with H292-shcontrol as a control) as well as A549-TIPE3$_{204aa}$ and A549-TIPE3$_{292aa}$ cells (with A549-mock as a control) (C) are shown. *, P<0.05, Student's *t*-test or ANOVA with LSD post-hoc multiple comparison, n=6 per group. (D,E) Tumorsphere assay. Representative images of tumor spheres (×200) (D) and the number of tumor spheres (E) are shown. *, P<0.05, Student's *t*-test or ANOVA with LSD post-hoc multiple comparison, n=6 per group. (F,G) Cell cycle analysis. Representative images of flow cytometric analysis of cell cycle (F) and percentage of each cell cycle phase distribution (G) are shown. *, P<0.05, Student's *t*-test or ANOVA with LSD post-hoc multiple comparison, n=6 per group. NSCLC, non-small cell lung cancer; CCK-8, Cell Counting Kit-8; ANOVA, analysis of variance; LSD, least significant difference.

migratory ability of H1299-shTIPE3 and H292-shTIPE3 tumor cells was markedly weakened (*P*<0.05) (*Figure 5A,B*). In contrast, the migratory ability of A549-TIPE3$_{204aa}$ and

A549-TIPE3$_{292aa}$ tumor cells was enhanced compared to that of A549-mock control cells (P<0.05) (*Figure 5A,B*). Moreover, knockdown of TIPE3 attenuated the invasion
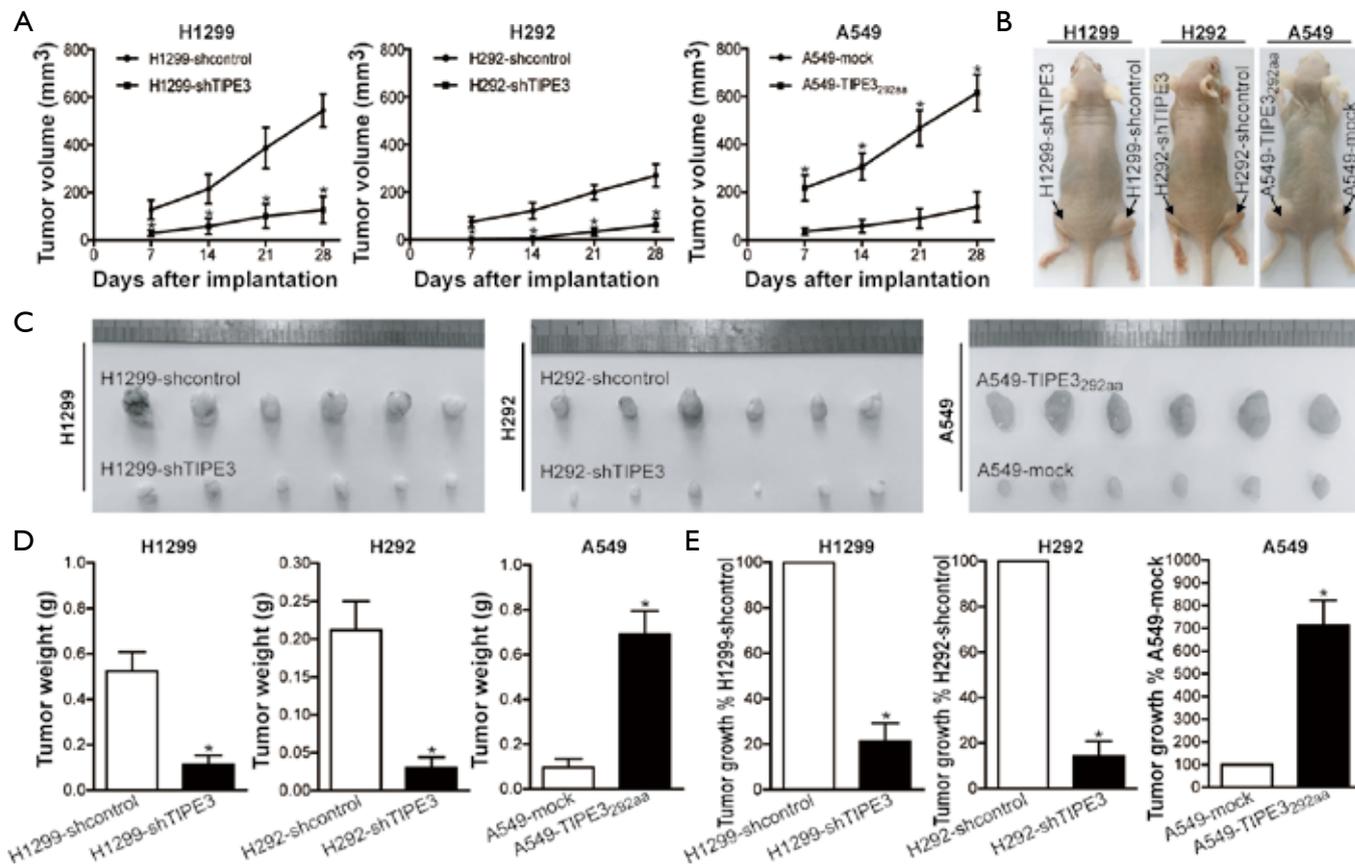
Figure 4 TIPE3 accelerates NSCLC cell growth *in vivo* in athymic nude mice. (A) Tumor volume. *, P<0.05, ANOVA with LSD post-hoc multiple comparison, n=6 per group. (B) Representative images of tumor-bearing mice. (C) Images of xenograft tumors. (D) Tumor weight. *, P<0.05, Student's *t*-test, n=6 per group. (E) *In vivo* relative growth ability. Relative growth ability of H1299-shTIPE3 cells (with H1299-shcontrol as a control), H292-shTIPE3 cells (with H292-shcontrol as a control), and A549-TIPE3$_{292aa}$ cells (with A549-mock as a control) calculated according to tumor weight. *, P<0.05, Student's *t*-test, n=6 per group. NSCLC, non-small cell lung cancer; ANOVA, analysis of variance; LSD, least significant difference.

ability of H1299 and H292 tumor cells, whereas TIPE3 overexpression promoted the invasion ability of A549 tumor cells (P<0.05) (*Figure 5C,D*). Our data showed that TIPE3 could promote the metastatic potential of human NSCLC cells.

TIPE3 promoted human NSCLC progression by modulating the AKT/ERK1/2-GSK3β-β-catenin/Snail axis

To investigate the molecular mechanism of TIPE3-exerted effects in NSCLC progression, the expression levels of proteins related to the AKT/ERK1/2-GSK3β-β-catenin/Snail signaling pathway were analyzed by WB in H1299-shTIPE3 *vs.* H1299-shcontrol, H292-shTIPE3 *vs.* H292-shcontrol, and A549-TIPE3$_{204aa}$ or

A549-TIPE3$_{292aa}$ *vs.* A549-mock tumor cells. As shown in *Figure 6A*, compared with H1299-shcontrol and H292-shcontrol control cells, the expression levels of p-AKT (T308), p-AKT (S473), p-ERK1/2, p-GSK3β, β-catenin, Snail1, and Slug were significantly decreased in H1299-shTIPE3 and H292-shTIPE3 tumor cells. Moreover, the expression levels of the abovementioned molecules were significantly higher in A549-TIPE3$_{204aa}$ and A549-TIPE3$_{292aa}$ tumor cells than in A549-mock control cells. More importantly, TIPE3 knockdown downregulated the nuclear levels of β-catenin, Snail1, and Slug in H1299 and H292 cells, but their nuclear levels were upregulated in TIPE3-overexpressing A549 cells (*Figure 6A*). Accordingly, knockdown of TIPE3 also upregulated the expression of E-cadherin but downregulated the expression of cyclin
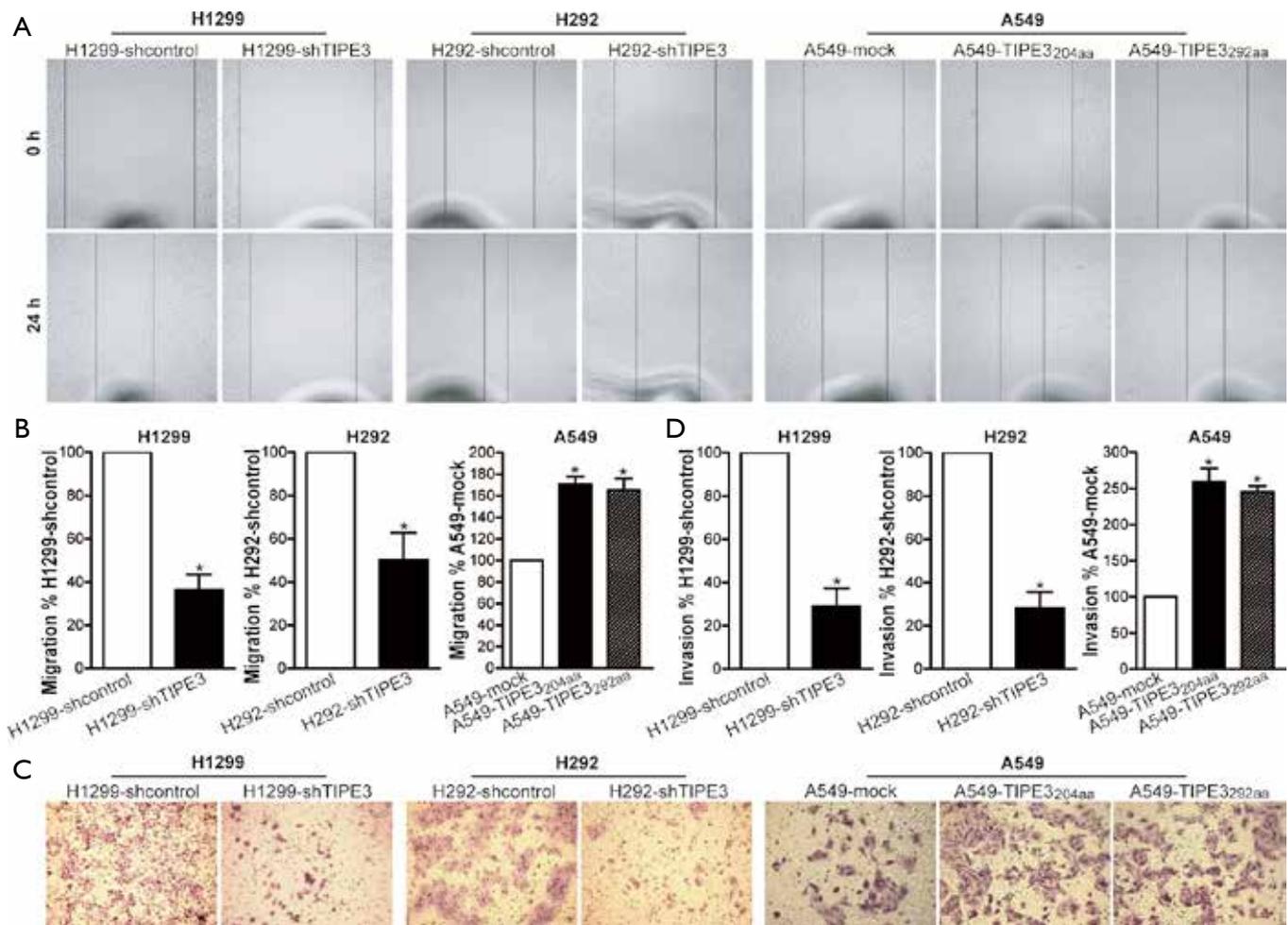
Figure 5 TIPE3 expedites NSCLC cell migration and invasion. (A,B) Wound healing assay. Representative images of wound healing assay (×100) (A) and relative migratory ability of H1299-shTIPE3 cells (with H1299-shcontrol as a control) and H292-shTIPE3 cells (with H292-shcontrol as a control) as well as A549-TIPE3$_{204aa}$ and A549-TIPE3$_{292aa}$ cells (with A549-mock as a control) (B) are shown. *, P<0.05, Student's *t*-test or ANOVA with LSD post-hoc multiple comparison, n=6 per group. (C,D) Transwell invasion assay. Representative images of Transwell invasion assay (×200) (C) and relative invasive ability of H1299-shTIPE3 cells (with H1299-shcontrol as a control) and H292-shTIPE3 cells (with H292-shcontrol as a control) as well as A549-TIPE3$_{204aa}$ and A549-TIPE3$_{292aa}$ cells (with A549-mock as a control) (D) are shown. *, P<0.05, Student's *t*-test or ANOVA with LSD post-hoc multiple comparison, n=6 per group. NSCLC, non-small cell lung cancer; ANOVA, analysis of variance; LSD, least significant difference.

D1, N-cadherin, and vimentin in H1299 and H292 cells, whereas overexpression of TIPE3 exerted the opposite effects in A549 tumor cells (*Figure 6A*). The *in vivo* effect of TIPE3 on the AKT/ERK1/2-GSK3β-β-catenin/Snail signaling pathway (*Figure 6B*) and its regulatory targets such as cyclin D1, E-cadherin, N-cadherin, and vimentin (data not shown) in H1299-shTIPE3 *vs.* H1299-shcontrol, H292-shTIPE3 *vs.* H292-shcontrol, and A549-TIPE3$_{292aa}$ *vs.* A549-mock NSCLC xenograft tumors was further

confirmed by IF analysis. Our results demonstrated that TIPE3 activated AKT and ERK1/2 signaling, promoted the phosphorylation of GSK3β at Ser9 and inactivated GSK3β activity, and enhanced the expression and transcriptional activity of β-catenin, Snail1, and Slug in human NSCLC cells.

To determine whether the AKT/ERK1/2-GSK3β pathway makes a critical contribution to TIPE3-induced upregulation of β-catenin, Snail1, and Slug in NSCLC
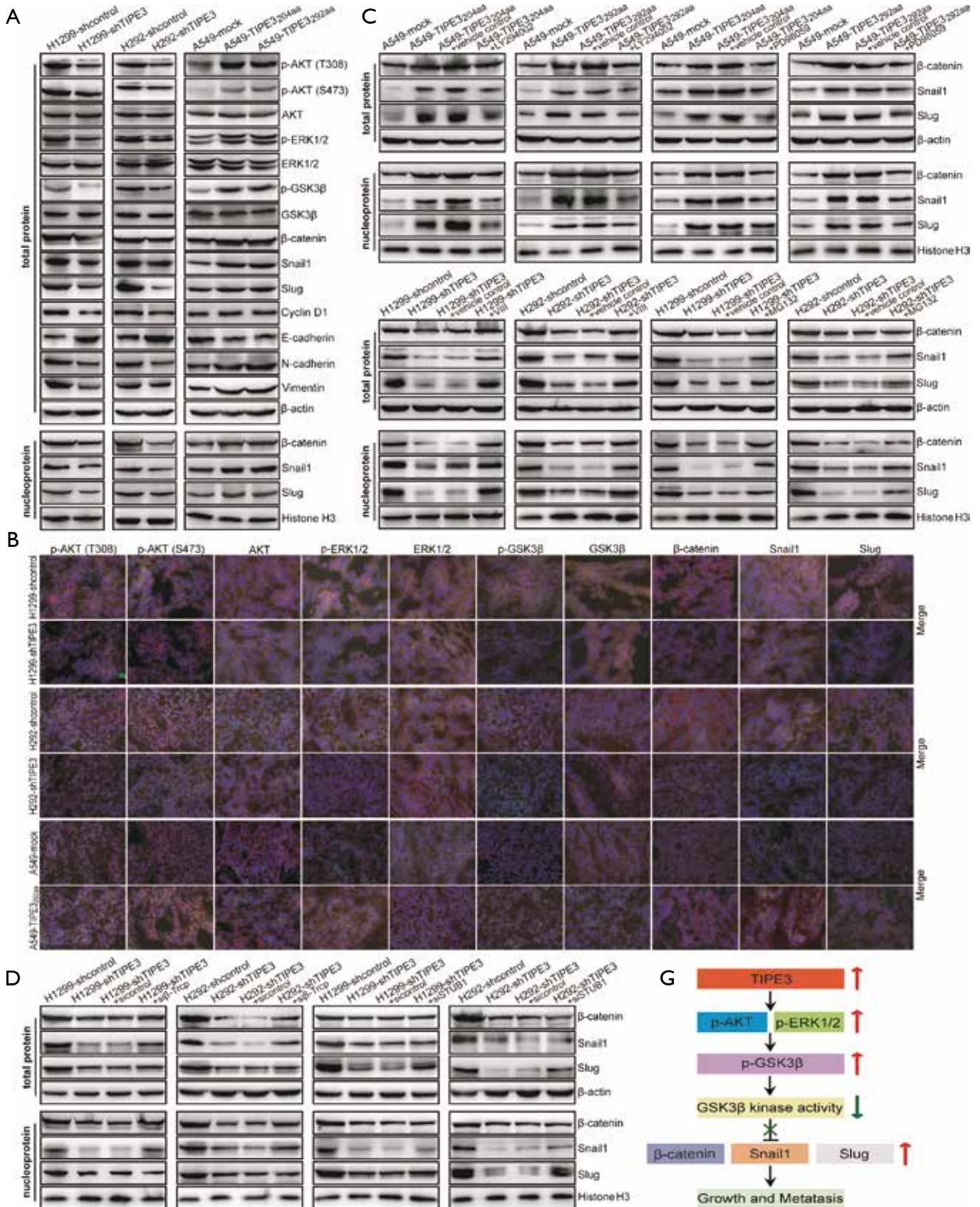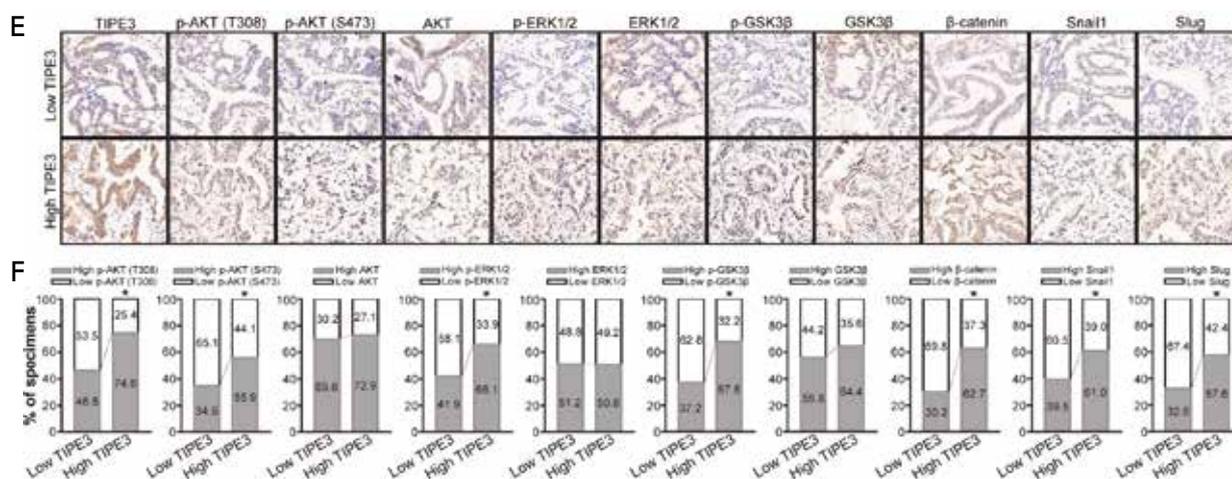
Figure 6 TIPE3 promotes NSCLC progression by an AKT/ERK1/2-GSK3β-β-catenin/Snail axis. (A) WB analysis of the AKT/ERK1/2-GSK3β-β-catenin/Snail axis and its regulatory targets in TIPE3 knock-down and TIPE3-overexpressing NSCLC cells. Representative WB images are shown. (B) IF analysis of the AKT/ERK1/2-GSK3β-β-catenin/Snail axis in TIPE3 knock-down and TIPE3-overexpressing NSCLC xenograft tumor tissues. Representative IF images of merge (red, Alexa Fluor 647; green, GFP; and blue, DAPI) (×200) are shown. (C) WB analysis of β-catenin, Snail1, and Slug in TIPE3-overexpressing NSCLC cells after treatment with PI3K or MEK inhibitor and TIPE3 knock-down NSCLC cells after treatment with GSK3β or proteasome inhibitor. Representative WB images are shown. (D) WB analysis of β-catenin, Snail1, and Slug in TIPE3 knock-down NSCLC cells after β-Trcp or STUB1 knockdown. Representative WB images are shown. (E,F) Clinical association of TIPE3 with the AKT/ERK1/2-GSK3β-β-catenin/Snail axis in lung cancer. Representative IHC images of Case 27 (+++, high TIPE3 expression) and Case 34 (-, low TIPE3 expression) lung cancer T tissues (×400) (E) are shown. Percentage of lung cancer T tissue specimens showing high or low TIPE3 expression in relation to the expression level of proteins related to the AKT/ERK1/2-GSK3β-β-catenin/Snail axis (F) is shown. *, P<0.05, Pearson's χ^2 test. (G) A schematic model for the mechanism of action of TIPE3 during NSCLC progression. Upregulation of TIPE3 promotes growth and metastasis in NSCLC cells by activating β-catenin, Snail1, and Slug transcriptional signaling via the AKT/ERK1/2-GSK3β axis. NSCLC, non-small cell lung cancer; WB: western blotting; AKT, protein kinase B; ERK1/2, extracellular signal-regulated kinase 1/2; GSK3β, glycogen synthase kinase 3β; IF, immunofluorescence; GFP, green fluorescent protein; DAPI: 4',6-diamidino-2-phenylindole; PI3K, phosphatidylinositol 3-kinase; MEK: mitogen-activated protein kinase kinase; IHC, immunohistochemistry; T, lung cancer tumor.

cells, we carried out PI3K/MEK/GSK3β kinase inhibition, proteasome inhibition, and E3 ubiquitin ligase β-Trcp or STUB1 siRNA assays. As shown in *Figure 6C*, inhibition of AKT or ERK1/2 signaling with LY294002 or PD98059 weakened TIPE3-induced upregulation of β-catenin, Snail1, and Slug expression in A549-TIPE3$_{204aa}$ and A549-TIPE3$_{292aa}$ cells, whereas inhibition of GSK3β or proteasome activity using VIII or MG132 abolished their TIPE3 knockdown-induced downregulation in H1299-shTIPE3 and H292-shTIPE3 cells. Notably, knockdown of β-Trcp and STUB1 in H1299-shTIPE3 and H292-shTIPE3 cells reversed the reduction of β-catenin or Snail1, and Slug caused by TIPE3 knockdown, respectively (*Figure 6D*). Our data showed that TIPE3 upregulated β-catenin, Snail1, and Slug in human NSCLC cells via the AKT/ERK1/2-GSK3β pathway in an ubiquitin-proteasome-dependent manner.

To examine whether there was a clinical association between TIPE3 and the AKT/ERK1/2-GSK3β-β-catenin/Snail signaling pathway in lung cancer T tissues, the expression of TIPE3 together with that of AKT/ERK1/2-GSK3β-β-catenin/Snail-related molecules was determined in a human lung cancer TMA by IHC (*Figure 6E*). As shown in *Figure 6F*, 74.6% (44 cases), 55.9% (33 cases), 66.1% (39 cases), 67.8% (40 cases), 62.7% (37 cases), 61.0% (36 cases), and 57.6% (34 cases) of cases with high TIPE3 expression (59 cases) showed a high level of p-AKT (T308), p-AKT (S473), p-ERK1/2, p-GSK3β, β-catenin, Snail1, and Slug, respectively. In contrast, only 46.5% (20 cases), 34.9% (15 cases), 41.9% (18 cases), 37.2% (16 cases), 30.2% (13 cases), 39.5% (17 cases), and 32.6% (14 cases) of cases with low TIPE3 expression (43 cases) exhibited a

high level of p-AKT (T308), p-AKT (S473), p-ERK1/2, p-GSK3β, β-catenin, Snail1, and Slug, respectively (P<0.05). In accordance with the cell model data, the clinical data of our study also revealed the expression level of TIPE3 to be positively correlated with the activation of the AKT/ERK1/2-GSK3β-β-catenin/Snail signaling pathway in lung cancer. Taken together, our findings suggest that the upregulation of TIPE3 promotes the growth and metastasis of human NSCLC cells substantially through activation of β-catenin, Snail1, and Slug transcriptional signaling via the AKT/ERK1/2-GSK3β axis (*Figure 6G*).

Discussion

Accumulating data have suggested that TIPE3 promotes the activation of the PI3K-AKT and MEK-ERK signaling pathways and displays pro-oncogenic activity in some types of cancer (7,8,10-13). The present study showed that the expression level of TIPE3 was upregulated in human lung cancer tissues and cell lines. High expression of TIPE3 was found to be closely associated with a large tumor size, a high pathologic stage, and the presence of lymph node metastasis in lung cancer patients. Loss- and gain-of-function experiments demonstrated that TIPE3 enhanced the malignant biological behaviors of human NSCLC cells. Mechanistic experiments revealed that TIPE3 upregulated β-catenin, Snail1, and Slug expression in NSCLC cells via the AKT/ERK1/2-GSK3β pathway in an ubiquitin-proteasome-dependent manner. TIPE3 expression was also demonstrated to be clinically correlated with the activation of the AKT/ERK1/2-GSK3β-β-catenin/Snail signaling pathway in human lung cancer tissues. Thus, our findings indicate that upregulation of TIPE3 promotes the progression of human NSCLC by activating β-catenin, Snail1, and Slug transcriptional signaling via the AKT/ERK1/2-GSK3β axis.

Human TIPE3 includes two transcript variants: NM_001311175.2 coding for 204aa (short TIPE3) and NM_207381.3 coding for 292aa (long TIPE3). It has been reported that both short and long TIPE3 has the ability to promote tumor cell growth and metastasis (10,13). Wang *et al.* (10) also demonstrated that N/C-terminal flag modification of TIPE3 affects the subcellular location of TIPE3, and the plasma membrane location of TIPE3 (TIPE3 with C-terminal flag) promotes growth and migration of NSCLC cells. Thus, we generated two recombinant LVs carrying TIPE3 204aa or 292aa CDS without fusion tags, and then established A549-TIPE3$_{204aa}$

and A549-TIPE3$_{292aa}$ transgenic NSCLC cell lines for gain-of-function assays. Consistent with the findings of previous reports (10,13), our data demonstrated that overexpression of TIPE3$_{204aa}$ and TIPE3$_{292aa}$ accelerated the proliferation and metastatic behavior of human NSCLC cells. Moreover, similar to Gao *et al.* (13), we found that overexpression of TIPE3$_{204aa}$ resulted in stronger pro-oncogenic activity than did overexpression of TIPE3$_{292aa}$, which may be partially attributable to the different expression efficiencies of TIPE3$_{204aa}$ and TIPE3$_{292aa}$ using the same expression system. As shown in our study, the level of TIPE3$_{204aa}$ in A549-TIPE3$_{204aa}$ cells was much higher than that of TIPE3$_{292aa}$ in A549-TIPE3$_{292aa}$ cells. Given the functional activity and expression levels of TIPE3$_{204aa}$ and TIPE3$_{292aa}$, the pro-oncogenic effect of TIPE3$_{292aa}$ may be more powerful than that of TIPE3$_{204aa}$. Nevertheless, WB analysis showed that TIPE3$_{292aa}$ was the main form of TIPE3 in lung cancer tissues and cell lines, indicating that the pathologically elevated expression of long TIPE3 but not short TIPE3 is a crucial causal factor of lung cancer progression. A previous study (10) demonstrated that in NSCLC, the expression of TIPE3 has no correlation with T stage or pathological grade, but the plasma membrane expression of TIPE3 is positively correlated with T stage; however, this is inconsistent with our data on the relationship between TIPE3 and the clinicopathological features of lung cancer patients in this study. To exclude the probability that this discrepancy may result from the analysis of different histologic types of lung cancer, we selected 99 NSCLC patients from the 102 lung cancer patients and analyzed the association of TIPE3 with their clinicopathological features. Our results (data not shown) also showed that the expression level of TIPE3 was positively correlated with large tumor size, high pathologic stage, and the presence of lymph node metastasis in NSCLC. Thus, the discrepancy between these studies is likely due to size differences between the specimens tested. Previous studies (12,13) have revealed a significant correlation between a high level of TIPE3 and poor prognosis in glioblastoma and gastric cancer. Therefore, the association of TIPE3 with the prognosis of lung cancer patients needs to be elucidated in our future research using the obtained follow-up survival data.

The PI3K-AKT (16,17) and MEK-ERK (18,19) signaling pathways are critical for cell proliferation, survival, apoptotic resistance, and motility, and their deregulation can lead to tumorigenesis and the development of various cell types. Aberrant activation of AKT and ERK1/2 signaling is commonly seen in lung cancer, and thus they can be served

as potentially therapeutic targets of lung cancer (20-22). TIPE3 has been found to facilitate activation of the PI3K-AKT and MEK-ERK pathways in both normal cells (8) and tumor cells, including lung cancer (8,10), breast cancer (11), and gastric cancer (13) cells. To illuminate the molecular mechanism underlying the oncogenic role of TIPE3 in NSCLC, we examined the effect of TIPE3 knockdown or overexpression on the expression levels of p-AKT and p-ERK1/2 in NSCLC cells. In our investigation, we demonstrated that TIPE3 potentiated the activation of AKT and ERK1/2 signaling in human NSCLC cells. The Wnt/β-catenin signaling pathway has important involvement in the regulation of diverse cellular and life processes such as cell proliferation, survival, differentiation, and motility, as well as stemness maintenance, embryonic development, and tissue homeostasis (23). Abnormal activation of β-catenin signaling has been shown to be closely associated with a wide range of human cancers and to promote cell cycle progression, metastasis, and cancer stem cell (CSC) self-renewal of cancer cells (24-26). When activated, as a crucial transcription cofactor, β-catenin translocates to the nucleus and subsequently binds with T cell factor (TCF) and lymphoid enhancer-binding factor T cell factor (LEF) transcription factors, resulting in transcription and expression of downstream target genes such as c-Myc, cyclin D1, and matrix metalloproteinase 7 (MMP7), and epithelial–mesenchymal transition (EMT)-related markers (23-26). EMT is a dynamic development process by which polarized epithelial cells lose their epithelial characteristics and acquire mesenchymal properties; this process is considered to be of critical importance in cancer metastasis, as it endows epithelial tumor cells with an enhanced migratory and invasive potential (27). Downregulation of the cell adhesion molecule E-cadherin and upregulation of mesenchymal molecules such as N-cadherin and vimentin are hallmarks of EMT (28). In addition to the modulatory role of β-catenin in the promotion of EMT, EMT transcription factors such as Snail1 and Slug (Snail2), which are master regulators of EMT, can induce EMT by transcriptionally repressing E-cadherin and activating N-cadherin and vimentin (29,30). Evidence has shown that upregulation of β-catenin (31,32), Snail1 (33), and Slug (34) plays a crucial role in carcinogenesis, aggressiveness, metastasis, therapeutic resistance, and poor survival in lung cancer. Activation of AKT and ERK1/2 signaling is frequently accompanied by the expression of β-catenin, Snail1, and Slug. Based on our findings that TIPE3 promotes the activation of AKT and

ERK1/2 signaling in NSCLC cells, we therefore further determined the total and nuclear levels of β-catenin, Snail1, and Slug as well as the levels of their targets including cyclin D1, E-cadherin, N-cadherin, and vimentin in TIPE3 knock-down or TIPE3-overexpressing NSCLC cells. As we expected, TIPE3 not only elevated the total and nuclear levels of β-catenin, Snail1, and Slug in NSCLC cells—it also upregulated cyclin D1, N-cadherin, and vimentin while downregulating E-cadherin. Our results conclusively demonstrate that TIPE3 is capable of strengthening the activation of AKT and ERK1/2 signaling and enhancing the expression and transcriptional activity of β-catenin, Snail1, and Slug in NSCLC cells, which may be an important mechanism for TIPE3-induced NSCLC progression.

GSK3β, which is a pleiotropic serine/threonine protein kinase, is constitutively active in resting epithelial cells. Its activity is positively regulated by phosphorylation at Tyr216 and negatively regulated by phosphorylation at Ser9 (35). GSK3β can be inactivated by various signaling mechanisms including the PI3K-AKT and MEK-ERK pathways (35-37). It has been reported that active AKT can directly phosphorylate Ser9 of GSK3β and suppress its activity (36). Active ERK1/2 has also been reported phosphorylate Thr43 of GSK3β and then promote ERK1/2-activated 90 kD ribosomal S6 kinase (p90RSK)-induced phosphorylation at Ser9, indirectly leading to the inhibition of GSK3β activity (37). Since TIPE3 activated AKT and ERK1/2 signaling in NSCLC cells, we speculated that TIPE3 would inactivate GSK3β in NSCLC cells. Therefore, we assessed the effect of TIPE3 on the level of p-GSK3β (Ser9), and found that TIPE3 upregulated p-GSK3β (Ser9) and inhibited the activity of GSK3β in human NSCLC cells. To clarify whether TIPE3-activated AKT and ERK1/2 signaling is accountable for TIPE3-mediated inactivation of GSK3β in NSCLC cells, we subsequently conducted PI3K and MEK kinase inhibition assays. We demonstrated that inhibition of AKT or ERK1/2 signaling suppressed the upregulation of p-GSK3β (Ser9) in TIPE3-overexpressing NSCLC cells (data not shown), indicating that TIPE3 decreases the activity of GSK3β in human NSCLC cells via the PI3K-AKT and MEK-ERK pathways. It has been demonstrated that active GSK3β can phosphorylate β-catenin (23), Snail1 (29,30,38,39), and Slug (40,41) and then promote their degradation by the ubiquitin-proteasome-dependent pathway. Conversely, inactive GSK3β can be in favor of the cytosolic and nuclear accumulation of β-catenin, Snail1, and Slug and then enhance their nuclear transcriptional signaling. It has also been demonstrated

that phosphorylation of β-catenin and Snail1 by GSK3β is specifically recognized and ubiquitylated by E3 ubiquitin ligase β-Trcp (23,38), whereas phosphorylation of Slug by GSK3β is recognized and ubiquitylated by STUB1 (41). Therefore, we predicted that TIPE3-elicited inactivation of GSK3β via AKT and ERK1/2 signaling would be involved in TIPE3-induced activation of β-catenin, Snail1, and Slug in NSCLC cells. By using inhibitors of PI3K/MEK/GSK3β kinase and proteasome as well as siRNAs targeting β-Trcp and STUB1, we showed that the TIPE3-activated AKT/ERK1/2-GSK3β signaling axis was indispensable in the inhibition of proteasome-induced degradation of β-catenin, Snail1, and Slug, and their accumulation in human NSCLC cells. Our data show that TIPE3 upregulates β-catenin, Snail1, and Slug in human NSCLC cells via the AKT/ERK1/2-GSK3β pathway in an ubiquitin-proteasome-dependent manner. Of note, ERK1/2 signaling has been found to transcriptionally activate the expression of Snail1 via the ETS-like gene 1 (ELK1)-early growth response 1 (EGR1) pathway (42-44). Hence, the present findings do not exclude the possibility that TIPE3 may also upregulate Snail1 at the transcription level by activation of the ERK1/2- ELK1-EGR1 pathway.

MYC (c-MYC) is a proto-oncogene transcription factor with highly conserved basic region/helix-loop-helix/leucine-zipper (bHLH-LZ) structure in the C-terminal region (45). MYC has been shown to be abnormally overexpressed in a variety of human cancers, and play an important role in inducing tumorigenesis, maintaining tumor growth and metabolism, stimulating tumor angiogenesis, and promoting tumor metastasis (46,47). It has been reported that β-catenin signaling can induce the transcriptional expression of MYC (24,25). It has also been shown that MEK-ERK and PI3K-AKT pathways can enhance the stability of MYC protein at the post-translational level by phosphorylating MYC Ser62, as well as inhibiting GSK3β-mediated phosphorylation of MYC Thr58 (45,48). These reports together with our results imply that TIPE3 also possibly promotes the expression of MYC, a key contributor to malignancy (49), in NSCLC cells via AKT/ERK1/2-GSK3β-β-catenin signaling, resulting in NSCLC progression. In addition, MYC as a powerful transcription factor can interact with co-regulatory factors MAX and MIZ1 to form MYC/MAX and MYC/MIZ1 heterodimers, thereby positively or negatively regulating the expression of many target genes (45). For example, tumor necrosis factor receptor superfamily member 10B (TNFRSF10B) has recently been found to be transcribed by MYC (50). Currently, the upstream regulatory mechanism for elevated expression of TIPE3 in human cancers remains largely illusive. Therefore, it is necessary to investigate the potential effect of MYC on the expression of TIPE3 in NSCLC cells in our future study. Furthermore, whether TIPE3-MYC double positive feedback loop would occur in NSCLC also needs to be addressed in the future.

In conclusion, our study has provided the first evidence that TIPE3-induced activation of AKT and ERK1/2 signaling followed by inactivation of GSK3β activity leads to the upregulation of β-catenin, Snail1, and Slug in human NSCLC cells. TIPE3 is capable of promoting human NSCLC progression via activation of β-catenin, Snail1, and Slug transcriptional signaling through the AKT/ERK1/2-GSK3β axis. Therefore, TIPE3 may represent a potential therapeutic target for NSCLC.

Footnote

Reporting Checklist: The authors have completed the MDAR reporting checklist. Available at http://dx.doi.org/10.21037/tlcr-21-147

Data Sharing Statement: Available at http://dx.doi.org/10.21037/tlcr-21-147

Conflicts of Interest: All authors have completed the ICMJE uniform disclosure form (available at http://dx.doi.org/10.21037/tlcr-21-147). RR serves as the Editor-in-Chief of *Translational Lung Cancer Research*. The other

authors have no conflicts of interest to declare.

References

1. Bray F, Ferlay J, Soerjomataram I, et al. Global cancer statistics 2018: GLOBOCAN estimates of incidence and mortality worldwide for 36 cancers in 185 countries. CA Cancer J Clin 2018;68:394-424.
2. Siegel RL, Miller KD, Jemal A. Cancer statistics, 2019. CA Cancer J Clin 2019;69:7-34.
3. Chen W, Zheng R, Baade PD. Cancer statistics in China, 2015. CA Cancer J Clin 2016;66:115-32.
4. Zappa C, Mousa SA. Non-small cell lung cancer: current treatment and future advances. Transl Lung Cancer Res 2016;5:288-300.
5. Niture S, Moore J, Kumar D. TNFAIP8: inflammation, immunity and human diseases. J Cell Immunol 2019;1:29-34.
6. Zhang L, Liu R, Luan YY, et al. Tumor necrosis factor-α induced protein 8: pathophysiology, clinical significance, and regulatory mechanism. Int J Biol Sci 2018;14:398-405.
7. Padmavathi G, Banik K, Monisha J, et al. Novel tumor necrosis factor-α induced protein eight (TNFAIP8/TIPE) family: functions and downstream targets involved in cancer progression. Cancer Lett 2018;432:260-71.
8. Fayngerts SA, Wu J, Oxley CL, et al. TIPE3 is the transfer protein of lipid second messengers that promote cancer. Cancer Cell 2014;26:465-78.
9. Moniz LS, Vanhaesebroeck B. A new TIPE of phosphoinositide regulator in cancer. Cancer Cell 2014;26:443-4.
10. Wang G, Guo C, Zhao H, et al. TIPE3 differentially modulates proliferation and migration of human non-small-cell lung cancer cells via distinct subcellular location. BMC Cancer 2018;18:260.
11. Lian K, Ma C, Hao C, et al. TIPE3 protein promotes breast cancer metastasis through activating AKT and NF-κB signaling pathways. Oncotarget 2017;8:48889-904.
12. Yuan F, Liu B, Xu Y, et al. TIPE3 is a regulator of cell apoptosis in glioblastoma. Cancer Lett 2019;446:1-14.
13. Gao JF, Zhang H, Lv J, et al. Effects of the long and short isoforms of TIPE3 on the growth and metastasis of gastric cancer. Biomed Pharmacother 2020;124:109853.
14. Fan Y, Shi Y, Lin Z et al. miR-9-5p suppresses malignant biological behaviors of human gastric cancer cells by negative regulation of TNFAIP8L3. Dig Dis Sci 2019;64:2823-9.
15. Qian F, Hu Q, Tian Y, et al. ING4 suppresses hepatocellular carcinoma via a NF- B/miR-155/FOXO3a signaling axis. Int J Biol Sci 2019;15:369-85.
16. Song M, Bode AM, Dong Z, et al. AKT as a therapeutic target for cancer. Cancer Res 2019;79:1019-31.
17. Fruman DA, Chiu H, Hopkins BD, et al. The PI3K pathway in human disease. Cell 2017;170:605-35.
18. Santamaria PG, Nebreda AR. Deconstructing ERK signaling in tumorigenesis. Mol Cell 2010;38:3-5.
19. Dhillon AS, Hagan S, Rath O, et al. MAP kinase signalling pathways in cancer. Oncogene 2007;26:3279-90.
20. Tan AC. Targeting the PI3K/Akt/mTOR pathway in non-small cell lung cancer (NSCLC). Thorac Cancer 2020;11:511-8.
21. Heigener DF, Gandara DR, Reck M. Targeting of MEK in lung cancer therapeutics. Lancet Respir Med 2015;3:319-27.
22. Ciuffreda L, Incani UC, Steelman LS, et al. Signaling intermediates (MAPK and PI3K) as therapeutic targets in NSCLC. Curr Pharm Des 2014;20:3944-57.
23. Nusse R, Clevers H. Wnt/β-catenin signaling, disease, and emerging therapeutic modalities. Cell 2017;169:985-99.
24. Zhan T, Rindtorff N, Boutros M. Wnt signaling in cancer. Oncogene 2017;36:1461-73.
25. Anastas JN, Moon RT. WNT signalling pathways as therapeutic targets in cancer. Nat Rev Cancer

2013;13:11-26.

26. Lecarpentier Y, Schussler O, Hébert JL, et al. Multiple targets of the canonical WNT/β-catenin signaling in cancers. Front Oncol 2019;9:1248.

27. Nieto MA, Huang RY, Jackson RA, et al. EMT: 2016. Cell 2016;166:21-45.

28. Zeisberg M, Neilson EG. Biomarkers for epithelial-mesenchymal transitions. J Clin Invest 2009;119:1429-37.

29. Lamouille S, Xu J, Derynck R. Molecular mechanisms of epithelial-mesenchymal transition. Nat Rev Mol Cell Biol 2014;15:178-96.

30. De Craene B, Berx G. Regulatory networks defining EMT during cancer initiation and progression. Nat Rev Cancer 2013;13:97-110.

31. Stewart DJ. Wnt signaling pathway in non-small cell lung cancer. J Natl Cancer Inst 2014;106:djt356.

32. Yang J, Chen J, He J, et al. Wnt signaling as potential therapeutic target in lung cancer. Expert Opin Ther Targets 2016;20:999-1015.

33. Wang G, Ma W, Li Y, et al. Prognostic value of Twist, Snail and E-cadherin expression in pathological N0 non-small-cell lung cancer: a retrospective cohort study. Eur J Cardiothorac Surg 2018;54:237-45.

34. Shih JY, Yang PC. The EMT regulator slug and lung carcinogenesis. Carcinogenesis 2011;32:1299-304.

35. Nagini S, Sophia J, Mishra R. Glycogen synthase kinases: Moonlighting proteins with theranostic potential in cancer. Semin Cancer Biol 2019;56:25-36.

36. Cross DA, Alessi DR, Cohen P, et al. Inhibition of glycogen synthase kinase-3 by insulin mediated by protein kinase B. Nature 1995;378:785-9.

37. Ding Q, Xia W, Liu JC, et al. Erk associates with and primes GSK-3beta for its inactivation resulting in upregulation of beta-catenin. Mol Cell 2005;19:159-70.

38. Zhou BP, Deng J, Xia W, et al. Dual regulation of snail by GSK-3beta-mediated phosphorylation in control of epithelial-mesenchymal transition. Nat Cell Biol 2004;6:931-40.

39. Yook JI, Li XY, Ota I, et al. A Wnt-Axin2-GSK3beta cascade regulates Snail1 activity in breast cancer cells. Nat Cell Biol 2006;8:1398-406.

40. Kim JY, Kim YM, Yang CH, et al. Functional regulation of Slug/Snail2 is dependent on GSK-3beta-mediated phosphorylation. FEBS J 2012;279:2929-39.

41. Kao SH, Wang WL, Chen CY, et al. GSK3β controls epithelial-mesenchymal transition and tumor metastasis by CHIP-mediated degradation of Slug. Oncogene 2014;33:3172-82.

42. Barberà MJ, Puig I, Dominguez D, et al. Regulation of Snail transcription during epithelial to mesenchymal transition of tumor cells. Oncogene 2004;23:7345-54.

43. Grotegut S, von Schweinitz D, Christofori G, et al. Hepatocyte growth factor induces cell scattering through MAPK/Egr-1-mediated upregulation of Snail. EMBO J 2006;25:3534-45.

44. Zhao J, Ou B, Han D, et al. Tumor-derived CXCL5 promotes human colorectal cancer metastasis through activation of the ERK/Elk-1/snail and AKT/GSK3β/β-catenin pathways. Mol Cancer 2017;16:70.

45. Kress TR, Sabò A, Amati B. MYC: connecting selective transcriptional control to global RNA production. Nat Rev Cancer 2015;15:593-607.

46. Dang CV. MYC on the path to cancer. Cell 2012;149:22-35.

47. Dejure FR, Eilers M. MYC and tumor metabolism: chicken and egg. EMBO J 2017;36:3409-20.

48. Sears R, Nuckolls F, Haura E, et al. Multiple Ras-dependent phosphorylation pathways regulate Myc protein stability. Genes Dev 2000;14:2501-14.

49. Chanvorachote P, Sriratanasak N, Nonpanya N. C-myc contributes to malignancy of lung cancer: a potential anticancer drug target. Anticancer Res 2020;40:609-18.

50. Chen W, Mou KY, Solomon P, et al. Large remodeling of the Myc-induced cell surface proteome in B cells and prostate cells creates new opportunities for immunotherapy. Proc Natl Acad Sci U S A 2021;118:e2018861118.